Nonequilibrium-induced metal-superconductor quantum phase transition in graphene

So Takei[1] and Yong Baek Kim[1,2]
[1]*Department of Physics, The University of Toronto, Toronto, Ontario M5S 1A7, Canada*
[2]*School of Physics, Korea Institute for Advanced Study, Seoul 130-722, Republic of Korea*
(Received 30 April 2008; revised manuscript received 12 September 2008; published 2 October 2008)

We study the effects of dissipation and time-independent nonequilibrium drive on an open superconducting graphene. In particular, we investigate how dissipation and nonequilibrium effects modify the semi-metal-BCS quantum phase transition that occurs at half filling in equilibrium graphene with attractive interactions. Our system consists of a graphene sheet sandwiched by two semi-infinite three-dimensional Fermi-liquid reservoirs, which act both as a particle pump/sink and a source of decoherence. A steady-state charge current is established in the system by equilibrating the two reservoirs at different but constant chemical potentials. The graphene sheet is described using the attractive Hubbard model in which the interaction is decoupled in the *s*-wave channel. The nonequilibrium BCS superconductivity in graphene is formulated using the Keldysh path-integral formalism, and we obtain generalized gap and number density equations valid for both zero and finite voltages. The behavior of the gap is discussed as a function of both attractive interaction strength and electron densities for various graphene-reservoir couplings and voltages. We discuss how tracing out the dissipative environment (with or without voltage) leads to decoherence of Cooper pairs in the graphene sheet, hence, to a general suppression of the gap order parameter at all densities. For weak enough attractive interactions we show that the gap vanishes even for electron densities away from half filling and illustrate the possibility of a dissipation-induced metal-superconductor quantum phase transition. We find that the application of small voltages does not alter the essential features of the gap as compared to the case when the system is subject to dissipation alone (i.e., zero voltage). The possibility of tuning the system through the metal-superconductor quantum critical point using voltage is presented.

DOI: 10.1103/PhysRevB.78.165401 PACS number(s): 03.65.Yz, 64.70.Tg, 74.78.−w

I. INTRODUCTION

The landmark experimental realization of an isolated graphite monolayer, or graphene,[1,2] has sparked intense theoretical and experimental interest in the material over the last few years.[3,4] A source of interest in the study of graphene is the unique properties of its charge carriers. At low energies, these charge carriers mimic relativistic particles and are most naturally described by the (2+1)-dimensional Dirac equation with an effective speed of light $c \sim v_F - 1 \times 10^6$ ms^{-1}. The fact that graphene is an excellent condensed-matter analog of (2+1)-dimensional quantum electrodynamics (QED) has been known to theorists for over 20 years.[5–7] However, it was not until the spectacular experimental realization of isolated graphene that experimentalists began observing signatures of the QED-type spectrum in their laboratories. Consequences of graphene's unique electronic properties have been revealed in the context of anomalous integer quantum-Hall effect[8,9] and minimum quantum conductivity in the limit of vanishing carrier concentrations.[8]

In addition to its importance in fundamental physics, graphene is expected to make a significant impact in the world of nanoscale electronics. Research efforts in developing graphene-based electronics have been fueled by a strong anticipation that it may supplement the silicon-based technology which is nearing its limits.[3] Graphene is a promising material for future nanoelectronics because of its exceptional carrier mobility which remains robustly high for a large range of temperatures, electric-field-induced concentrations,[1,2,8,9] and chemical doping.[10] Indeed, recent experiments have explored the possibilities of in-plane graphene heterostructures by engineering arbitrary spatial density variation using local gates.[11–13] The application of local-gate techniques to graphene marks an important first step on the road toward graphene-based electronics.

From a theoretical point of view we realize that graphene nanoelectronics requires a theoretical understanding of open nonequilibrium graphene. Naturally, graphene in nanocircuits is subject to decoherence effects due to its coupling to external leads via tunnel junctions. Furthermore, a nonequilibrium treatment of graphene becomes necessary when a charge current is driven through it. To this date, effects of dissipation and nonequilibrium drive on graphene electronic properties have not been addressed. The focus of this paper is to show a theoretical framework in which these effects can be studied and illustrate how they give rise to striking influences on the equilibrium properties of graphene.

This work considers dissipation and nonequilibrium effects on superconducting graphene. Beside the possibility of superconductivity in graphene by proximity effect,[14] some works suggested the potential of achieving plasmon-mediated singlet superconductivity in graphene.[15,16] Several groups have investigated the equilibrium mean-field theory of superconductivity in graphene using the attractive Hubbard model on the honeycomb lattice. Uchoa and Castro Neto[15] studied spin singlet superconductivity in graphene at various fillings by considering both the usual *s*-wave pairing as well as pairing with $p+ip$ orbital symmetry permitted by graphene's honeycomb lattice structure. Zhao and Paramekanti[17] examined the possibility of *s*-wave superconductivity on the honeycomb lattice. Both works show that (in the absence of *p*-wave pairing) half-filled graphene displays a semi-metal-superconductor quantum critical point at a fi-

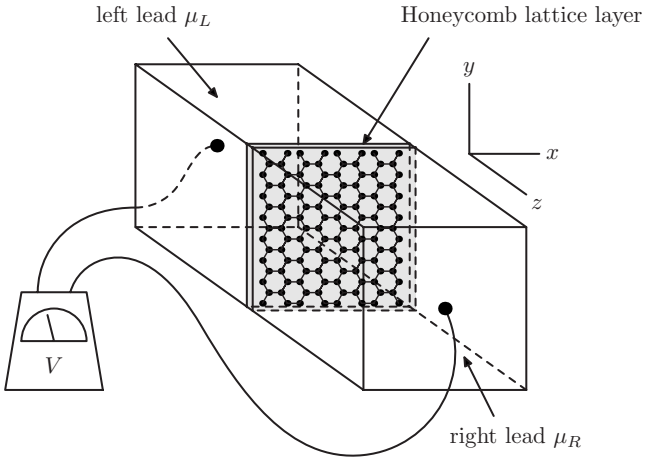

FIG. 1. A schematic of the system considered. Chemical potential mismatch in the two leads will lead to a charge current parallel to the z axis.

nite critical attractive interaction strength u_c. Away from half filling, the system exhibits Cooper instability at any finite u and thus undergoes the usual BCS-BEC (Bose-Einstein condensate) crossover as u is increased. The difficulty in achieving superconductivity at half filling is a result of the vanishing density of states at the Dirac point and the absence of electron screening.

In this work, the superconducting graphene sheet is subjected to dissipation and nonequilibrium drive by coupling it to two semi-infinite particle reservoirs via tunnel junctions. The geometry of the system is shown in Fig. 1. While the two reservoirs are independently held in thermal and chemical equilibriums at all times, an out-of-plane steady-state current through graphene is established by equilibrating the reservoirs at two different but constant chemical potentials. The leads act as infinite reservoirs and are assumed to be held at a common temperature T at all times. Nonequilibrium theory of BCS superconductivity is formulated using the Keldysh path-integral formalism, and the resulting nonequilibrium mean-field equations are used to investigate the gap behavior at and near half filling for various attractive interaction strengths. The zero-temperature gap phase diagram in the parameter space of filling n and the interaction strength u is particularly interesting due to the survival of the semimetallic phase at half filling. The main goal of this work is to investigate the fate of this phase in the presence of dissipation and nonequilibrium current, and our results can be directly compared to the gap phase diagram in Fig. 2 of the work of Zhao and Paramekanti.[17]

Our main results are now qualitatively summarized. We find that the gap is generally suppressed in the presence of the leads. As this paper will discuss in detail, the key to understanding our findings is to notice that the dissipation of electrons into the leads acts as a pair-breaking mechanism for the Cooper pairs in the central graphene sheet. This mechanism, hence the suppression, is present at both zero and finite voltages and for all electron densities. As a consequence, the Fermi-liquid ground state of the system remains stable against Cooper pairing up to some density-dependent finite attractive interaction strength $u_c(n)$ at all densities.

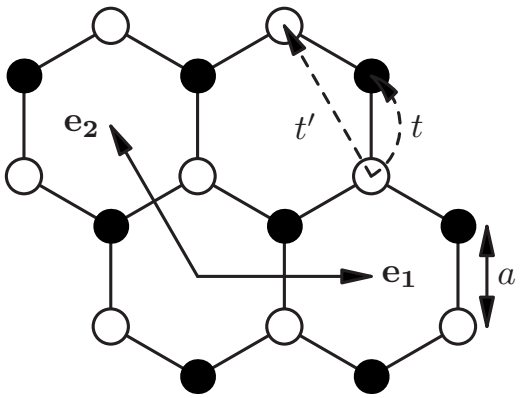

FIG. 2. Graphene honeycomb lattice. $\mathbf{e}_1$ and $\mathbf{e}_2$ are the unit-cell basis vectors of graphene with lattice constant $\sqrt{3}a \approx 2.46$ Å ($a \approx 1.42$ Å). A unit cell contains two carbon atoms belonging to the two sublattices A (white circles) and B (black circles). All nearest- and next-nearest-neighbor hopping matrix elements are $-t$ and $-t'$, respectively.

With respect to the gap phase diagram, dissipation gives rise to a finite region around half filling in which the gap vanishes (see Fig. 5). From these results, we infer that dissipation induces a metal-superconductor quantum phase transition at all fillings, for which the tuning parameter is the attractive interaction strength u. The qualitative behavior of the gap is not greatly different in both the zero and finite voltage cases as long as the voltage is small, i.e., $V \ll \Gamma$, where Γ denotes the average tunneling rate of electrons between graphene and the two leads. However, we stress the possibility of tuning the system across the dissipation-induced metal-superconductor quantum phase transition using voltage. The significance lies in the fact that voltage introduces a different means of tuning the system across the transition in addition to a more difficult approach of adjusting the attractive interaction strength.

This paper is organized as follows. In Sec. II, we introduce the Hamiltonian which models our heterostructure. The mean-field treatment of the model is formulated on the Keldysh contour in Sec. III. In Sec. III B, the nonequilibrium gap and number density equations will be derived. The results are presented in Sec. IV. The effects of dissipation in the absence of voltage is discussed in Sec. IV A while the finite voltage effects are included in Sec. IV B. We conclude in Sec. V.

II. MODEL

The lead-graphene-lead heterostructure considered in this work is shown in Fig. 1. Graphene is located on the $z=0$ plane, and each of its sites is labeled using two coordinates $\mathbf{r}_i=(x_i,y_i,z_i\equiv 0)$. The semi-infinite metallic leads extend from both sides of the graphene sheet for $z>0$ and $z<0$. We assume that the leads are separated from graphene by thin insulating barriers and the tunneling of electrons through each of the barriers can be described by phenomenological tunneling parameters. Full translational symmetry is present along the planes parallel to the xy plane for $z\neq 0$ while only

the discrete translational symmetry of the graphene lattice is present at $z=0$. The leads are assumed to be in thermal equilibrium with their continuum of states occupied according to the Fermi-Dirac distribution $f_\alpha(\omega)=\{1+\exp[\beta(\omega-\mu_\alpha)]\}^{-1}$, where $\alpha=L$(left) and R(right) label the leads. An electric potential bias is set up in the out-of-plane direction by tuning the chemical potentials of the leads to different values.

The Hamiltonian consists of three parts,

$$H = H_{\text{sys}} + H_{\text{res}} + H_{\text{sys-res}}. \tag{1}$$

The central graphene sheet is modeled using the attractive Hubbard model on the honeycomb lattice. The kinetic term is a tight-binding description for the π orbitals of carbon that includes nearest- and next-nearest-neighbor hopping processes. The on-site interaction strength is parametrized by U. The Hamiltonian for the layer is

$$H_{\text{sys}} = -t\sum_{\langle i,j\rangle,\sigma}(c^\dagger_{i,\sigma}c_{j,\sigma}+\text{H.c.}) - t'\sum_{\langle\langle i,j\rangle\rangle,\sigma}(c^\dagger_{i,\sigma}c_{j,\sigma}+\text{H.c.}) - U\sum_i c^\dagger_{i,\uparrow}c^\dagger_{i,\downarrow}c_{i,\downarrow}c_{i,\uparrow}. \tag{2}$$

$c^\dagger_{i,\sigma}$ ($c_{i,\sigma}$) creates (annihilates) electrons on site $\mathbf{r}_i$ of the graphene honeycomb lattice with spin $\sigma(\sigma=\uparrow,\downarrow)$. U is assumed positive due to attractive interaction, and t and t' are the nearest- and next-nearest-neighbor hopping parameters, respectively. Specific values for t and t' have been estimated[18] by comparing a tight-binding description to first-principles calculations. Following their estimates, we take $t=2.7$ eV and fix $t'/t=0.04$.

The honeycomb lattice can be described in terms of two interpenetrating triangular sublattices A and B (see Fig. 2). Each unit cell is composed of two atoms, each one of types A and B. Primitive translation vectors, $\mathbf{e}_1$ and $\mathbf{e}_2$, are

$$\mathbf{e}_1=(\sqrt{3},0)\mathbf{e}_2=(-\sqrt{3}/2,3/2)\mathbf{e}_3=\mathbf{e}_1+\mathbf{e}_2, \tag{3}$$

where they are expressed in units of a, which is the distance between two nearest carbon atoms. Any A atom is connected to its nearest neighbors on the B lattice by three vectors,

$$\mathbf{d}_1=(0,1),$$

$$\mathbf{d}_2=(-\sqrt{3}/2,-1/2),$$

$$\mathbf{d}_3=(\sqrt{3}/2,-1/2). \tag{4}$$

In momentum space, the kinetic term reads

$$H^K_{\text{sys}} = \frac{1}{N_\Delta}\sum_{\mathbf{k},\sigma}(a^\dagger_{\mathbf{k},\sigma}\ b^\dagger_{\mathbf{k},\sigma})\begin{pmatrix}\lambda_{\mathbf{k}} & g^*_{\mathbf{k}}\\ g_{\mathbf{k}} & \lambda_{\mathbf{k}}\end{pmatrix}\begin{pmatrix}a_{\mathbf{k},\sigma}\\ b_{\mathbf{k},\sigma}\end{pmatrix}, \tag{5}$$

where

$$\lambda_{\mathbf{k}} = -t'\left(\sum_{i=1}^{3}e^{i\mathbf{k}\cdot\mathbf{e}_i}+\text{c.c.}\right), \tag{6}$$

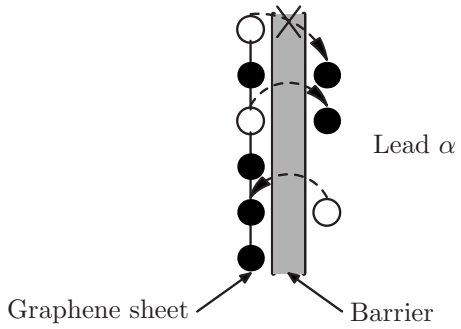

FIG. 3. A diagram illustrating the type of tunneling processes that are considered in this work. The diagram is an edge-on view of the interface between the graphene sheet and a lead. The only tunneling events that are allowed are those in which the (x,y) coordinates of electrons remain unaltered. Thus, while the lower two processes in the diagram are allowed, tunneling of the type shown at the top is disallowed.

$$g_{\mathbf{k}} = -t\sum_{i=1}^{3}e^{i\mathbf{k}\cdot\mathbf{d}_i}. \tag{7}$$

Components of the pseudospinor, $a^\dagger_{\mathbf{k},\sigma}$ and $b^\dagger_{\mathbf{k},\sigma}$, describe quasiparticles that belong to sublattices A and B, respectively. Here, N_Δ denotes the number of lattice sites in a triangular sublattice. $N=2N_\Delta$ will denote the total number of sites on the honeycomb lattice.

Coupling between leads and the graphene sheet is modeled using the following Hamiltonian:

$$H_{\text{sys-res}} = \int\frac{dk_z}{2\pi}\sum_{\alpha=L,R}\sum_{i,\sigma}\zeta_\alpha(C^\dagger_{i,\sigma,\alpha,k_z}c_{i,\sigma}+\text{H.c.}). \tag{8}$$

ζ_α is a phenomenological tunneling matrix that describes the tunneling of an electron between site i on the graphene sheet and an adjacent site on lead α (see Fig. 3). We only consider lead-graphene tunneling processes in which (x,y) coordinates of the electron in the initial and final states are the same. This assumption simplifies various computational steps without altering the qualitative features of the final results. $C^\dagger_{i,\sigma,\alpha,k_z}$ creates an electron in lead α at coordinates (x_i,y_i) with spin σ and longitudinal momentum k_z. We assume here that the tunneling parameters are independent of frequency and momentum but maintain their lead dependence in order to describe possible asymmetries in the lead-layer couplings. In momentum space, the tunneling Hamiltonian in Eq. (8) becomes

$$H_{\text{sys-res}} = \sum_\alpha\zeta_\alpha\int\frac{dk_z}{2\pi}\frac{1}{N_\Delta}\sum_{\mathbf{k},\sigma} \times(A^\dagger_{\mathbf{k},k_z,\sigma,\alpha}a_{\mathbf{k},\sigma}+B^\dagger_{\mathbf{k},k_z,\sigma,\alpha}b_{\mathbf{k},\sigma}+\text{H.c.}). \tag{9}$$

The in-plane momentum, $\mathbf{k}$, is the component of momentum parallel to the graphene plane and the out-of-plane momentum, k_z, is its component normal to the plane. $A^\dagger_{\mathbf{k},k_z,\sigma,\alpha}$ ($B^\dagger_{\mathbf{k},k_z,\sigma,\alpha}$) corresponds to an electron mode propagating in "sublattice $A(B)$" in lead α with spin σ and wave vector $\mathbf{k}$. Although the full in-plane translational symmetry of the

leads implies that $\mathbf{k}$ can take on any value in $\mathbb{R}^2$, the tunneling assumption (see Fig. 3) tells us that the only modes that tunnel are those with $\mathbf{k}$ values that are the allowed modes of the triangular sublattices in the graphene sheet. All other inconsequential modes can eventually be integrated out in the path-integral sense and will merely contribute a multiplicative factor in front of the partition function. Therefore, we will not consider these modes further.

Because graphene is an atomically thin two-dimensional material, an electron may tunnel from one lead to the other without scattering within the graphene sheet. However, we expect the amplitude of this direct tunneling between the leads to be smaller in comparison to the considered lead-layer coupling since the former involves tunneling through two tunnel barriers as opposed to one. For this reason, direct tunneling processes will not be considered in this work.

Both leads are assumed to be Fermi liquids,

$$H_{\mathrm{res}} = \sum_{\alpha,\Lambda} \frac{1}{N_\Delta} \int \frac{dk_z}{2\pi} \sum_{\mathbf{k},k_z,\sigma} \epsilon_{\mathbf{k},k_z} \times (A^\dagger_{\mathbf{k},k_z,\sigma,\alpha} A_{\mathbf{k},k_z,\sigma,\alpha} + B^\dagger_{\mathbf{k},k_z,\sigma,\alpha} B_{\mathbf{k},k_z,\sigma,\alpha}), \tag{10}$$

with a separable dispersion

$$\epsilon_{\mathbf{k},k_z} = \epsilon_{\mathbf{k}} + \epsilon_{k_z} = \frac{|\mathbf{k}|^2}{2m_e} + \frac{k_z^2}{2m_e}. \tag{11}$$

Beside their role as a particle pump/sink, the leads play an important role as a heat sink. An important assumption we make is that any heat generated in the interacting region due to the application of a transverse electric field is efficiently dissipated into the leads so as to prevent build up of heat in the region. This is a well-justified assumption because the leads are assumed to be infinite and the interacting region has a thin profile.

In equilibrium ($\mu_{\mathrm{res}} = \mu_R = \mu_L$), the central system is expected to reach chemical equilibrium with the reservoirs in the long-time limit so that $\mu_{\mathrm{sys}} = \mu_{\mathrm{res}}$. In the out-of-equilibrium case, the system is coupled to two reservoirs that are not in chemical equilibrium. Therefore, although the electron distribution in the interacting system reaches a static form in the long-time limit, it is in no way expected to have an equilibrium form due to constant influx (outflux) of particles from (into) the leads.

III. KELDYSH PATH INTEGRAL FORMULATION

In this section, we formulate a theory of nonequilibrium BCS superconductivity in graphene using the Keldysh functional-integral formalism. The theory is first expressed in terms of a Keldysh partition function using coherent states of fields defined on the time-loop Keldysh contour $\mathcal{C}$. Following a Hubbard-Stratonovic decoupling of the quartic interaction term in the pair channel, a BCS theory for superconducting graphene is obtained by assuming a static homogeneous gap integrating out both leads and graphene electrons and extremizing the effective action with respect to the gap. The resulting mean-field equations, which are a nonequilibrium generalization of the corresponding equilibrium equations,[17] are analyzed in the remainder of this paper.

The starting Keldysh generating functional reads

$$Z^K = \int \mathcal{D}\{a,\bar{a},b,\bar{b},A,\bar{A},B,\bar{B}\} e^{iS^K}, \tag{12}$$

where

$$S^K = S^K_{\mathrm{sys}} + S^K_{\mathrm{res}} + S^K_{\mathrm{sys\text{-}res}}. \tag{13}$$

If we introduce four-component spinors defined in Nambu-sublattice space for both graphene and leads electrons,

$$\phi_{\mathbf{k}}(t) \equiv \begin{pmatrix} a_{\mathbf{k},\uparrow}(t) \\ \bar{a}_{-\mathbf{k},\downarrow}(t) \\ b_{\mathbf{k},\uparrow}(t) \\ \bar{b}_{-\mathbf{k},\downarrow}(t) \end{pmatrix}, \tag{14}$$

$$\Phi_{\mathbf{k},\mathbf{k_z},\alpha}(t) \equiv \begin{pmatrix} A_{\mathbf{k},\mathbf{k_z},\uparrow,\alpha}(t) \\ -\bar{A}_{-\mathbf{k},-\mathbf{k_z},\downarrow,\alpha}(t) \\ B_{\mathbf{k},\mathbf{k_z},\uparrow,\alpha}(t) \\ -\bar{B}_{-\mathbf{k},-\mathbf{k_z},\downarrow,\alpha}(t) \end{pmatrix}, \tag{15}$$

the actions in Eq. (13) become

$$S^K_{\mathrm{sys}} = \int_{\mathcal{C}} dt \frac{1}{N_\Delta} \sum_{\mathbf{k}} \bar{\phi}_{\mathbf{k}}(t)[i\partial_t - \lambda_{\mathbf{k}} \tau^N_z - g_{\mathbf{k}} \tau^N_z \tau^\Lambda_- - g^*_{\mathbf{k}} \tau^N_z \tau^\Lambda_+] \phi_{\mathbf{k}}(t) + U \int_{\mathcal{C}} dt \sum_i [\bar{a}_{i,\uparrow}(t)\bar{a}_{i,\downarrow}(t)a_{i,\downarrow}(t)a_{i,\uparrow}(t) + \bar{b}_{i,\uparrow}(t)\bar{b}_{i,\downarrow}(t)b_{i,\downarrow}(t)b_{i,\uparrow}(t)], \tag{16}$$

$$S^K_{\mathrm{res}} = \int_{\mathcal{C}} dt \int \frac{dk_z}{2\pi} \sum_\alpha \frac{1}{N_\Delta} \sum_{\mathbf{k}} \bar{\Phi}_{\mathbf{k},\mathbf{k_z},\alpha}(t)(i\partial_t - \epsilon_{\mathbf{k},k_z} \tau^N_z) \Phi_{\mathbf{k},\mathbf{k_z},\alpha}(t), \tag{17}$$

and

$$S^K_{\mathrm{sys\text{-}res}} = \int_{\mathcal{C}} dt \int \frac{dk_z}{2\pi} \sum_\alpha \zeta_\alpha \frac{1}{N_\Delta} \sum_{\mathbf{k}} \times [\bar{\Phi}_{\mathbf{k},\mathbf{k_z},\alpha}(t)\phi_{\mathbf{k}}(t) + \bar{\phi}_{\mathbf{k}}(t)\Phi_{\mathbf{k},\mathbf{k_z},\alpha}(t)]. \tag{18}$$

$\tau^\nu_\pm$ are 2×2 matrices given by

$$\tau^\nu_\pm = \frac{1}{2}(\tau^\nu_x \pm i\tau^\nu_y), \tag{19}$$

where $\tau^\nu_{x,y,z}$ are Pauli matrices. Superscript ν indicates the space in which the matrices act; Λ (N) denotes sublattice (Nambu) space. The quartic interaction term in Eq. (16) is decoupled using Hubbard-Stratonovic fields $\Delta^A_i(t)$ and $\Delta^B_i(t)$. In the BCS mean-field approximation, where this field is assumed static and homogeneous (i.e., $\Delta^A_i(t) = \Delta^B_i(t) \equiv \Delta$), the resulting action of the system reads

$$S_{\rm sys}^K = \int_C dt \frac{1}{N_\Delta} \sum_{\mathbf{k}} \bar{\phi}_{\mathbf{k}}(t)[i\partial_t - \lambda_{\mathbf{k}}\tau_z^N - g_{\mathbf{k}}\tau_z^N\tau_-^\Lambda - g_{\mathbf{k}}^*\tau_z^N\tau_+^\Lambda + U\Delta\tau_+^N + U\Delta^*\tau_-^N]\phi_{\mathbf{k}}(t) - 2U|\Delta|^2. \tag{20}$$

The self-consistency condition for the gap is

$$\Delta = \langle a_{i,\downarrow}a_{i,\uparrow}\rangle(t) = \langle b_{i,\downarrow}b_{i,\uparrow}\rangle(t). \tag{21}$$

The time-loop contour integral is carried out by first splitting every field into two components, labeled as "+" and "−," which reside on the forward and the backward parts of the time contour, respectively.[19–21] The continuous action then becomes

$$S^K = \int_{-\infty}^{\infty} dt[\mathcal{L}_+(t) - \mathcal{L}_-(t)], \tag{22}$$

where $\mathcal{L}_\pm(t)$ is the Lagrangian corresponding to the action defined in Eq. (13) written in terms of + (−) fields. When time-ordered products of Heisenberg fields in the theory are constructed on the Keldysh contour, we obtain four Green's functions,

$$iG^T(t,t') = \langle \Upsilon_+(t)\bar{\Upsilon}_+(t')\rangle,$$

$$iG^{\tilde{T}}(t,t') = \langle \Upsilon_-(t)\bar{\Upsilon}_-(t')\rangle,$$

$$iG^<(t,t') = \langle \Upsilon_+(t)\bar{\Upsilon}_-(t')\rangle,$$

$$iG^>(t,t') = \langle \Upsilon_-(t)\bar{\Upsilon}_+(t')\rangle.$$

Because these Green's functions are not linearly independent, a linear transformation of the fields from the Kadanoff-Baym basis (+,−) to the Keldysh basis (cl and q for bosons; 1 and 2 for fermions) is commonly performed. For bosons, the barred fields are related to the unbarred fields simply by complex conjugation, and thus, the transformation is identical for both,

$$\begin{pmatrix} \Upsilon_{cl} \\ \Upsilon_q \end{pmatrix} = \frac{1}{\sqrt{2}}\begin{pmatrix} 1 & 1 \\ 1 & -1 \end{pmatrix}\begin{pmatrix} \Upsilon_+ \\ \Upsilon_- \end{pmatrix}. \tag{23}$$

For fermions, unbarred fields are transformed in the same manner as Eq. (23). For barred fields, we choose a different transformation,[19]

$$\begin{pmatrix} \bar{\Upsilon}_1 \\ \bar{\Upsilon}_2 \end{pmatrix} = \frac{1}{\sqrt{2}}\begin{pmatrix} 1 & -1 \\ 1 & 1 \end{pmatrix}\begin{pmatrix} \bar{\Upsilon}_+ \\ \bar{\Upsilon}_- \end{pmatrix}. \tag{24}$$

In order to express the Keldysh action [Eq. (22)] in the Keldysh basis it is now appropriate to define eight-component spinors for graphene and leads electrons defined in the Nambu-sublattice-Keldysh space. Since we are interested in steady-state properties of the system, it is useful to first Fourier transform the fields into frequency space. We define the eight-component spinors as

$$\psi_k \equiv \begin{pmatrix} a_{k,\uparrow}^1 \\ \bar{a}_{-k,\downarrow}^1 \\ b_{k,\uparrow}^1 \\ \bar{b}_{k,\downarrow}^1 \\ a_{k,\uparrow}^2 \\ \bar{a}_{-k,\downarrow}^2 \\ b_{k,\uparrow}^2 \\ \bar{b}_{-k,\downarrow}^2 \end{pmatrix} \Psi_{k,k_z,\alpha} \equiv \begin{pmatrix} A_{k,k_z,\uparrow,\alpha}^1 \\ -\bar{A}_{-k,-k_z,\downarrow,\alpha}^1 \\ B_{k,k_z,\uparrow,\alpha}^1 \\ -\bar{B}_{-k,-k_z,\downarrow,\alpha}^1 \\ A_{k,k_z,\uparrow,\alpha}^2 \\ -\bar{A}_{-k,-k_z,\downarrow,\alpha}^2 \\ B_{k,k_z,\uparrow,\alpha}^2 \\ -\bar{B}_{-k,-k_z,\downarrow,\alpha}^2 \end{pmatrix}, \tag{25}$$

where $k \equiv (\mathbf{k},\omega)$ is the energy-momentum three vector. The action [Eq. (22)] then becomes

$$S_{\rm sys}^K = \int_k \bar{\psi}_k\{[g_0^R(k)\tau_\uparrow^N - g_0^R(-k)\tau_\downarrow^N]\tau_\uparrow^K[g_0^A(k)\tau_\uparrow^N - g_0^A(-k)\tau_\downarrow^N]\tau_\downarrow^K + g_0^K(k)\tau_\uparrow^N\tau_+^K + g_0^K(k)\tau_\downarrow^N\tau_-^K - g_{\mathbf{k}}\tau_z^N\tau_-^\Lambda - g_{\mathbf{k}}^*\tau_z^N\tau_+^\Lambda + U[\Delta_q\tau_+^N + \Delta_q^*\tau_-^N + (\Delta_{cl}\tau_+^N + \Delta_{cl}^*\tau_-^N)\tau_x^K]\}\psi_k - 2U[\Delta_{cl}^*\Delta_q + \Delta_q^*\Delta_{cl}], \tag{26}$$

$$S_{\rm res}^K = \int_k \int \frac{dk_z}{2\pi}\sum_\alpha \bar{\Psi}_{k,k_z,\alpha}\{[\tilde{g}_\alpha^R(k)\tau_\uparrow^N - \tilde{g}_\alpha^R(-k)\tau_\downarrow^N]\tau_\uparrow^K \times[\tilde{g}_\alpha^A(k)\tau_\uparrow^N - \tilde{g}_\alpha^A(-k)\tau_\downarrow^N]\tau_\downarrow^K + \tilde{g}_\alpha^K(k)\tau_\uparrow^N\tau_+^K + \tilde{g}_\alpha^K(k)\tau_\downarrow^N\tau_-^K\}\Psi_{k,k_z,\alpha}, \tag{27}$$

and

$$S_{\rm sys\text{-}res}^K = \int_k \int \frac{dk_z}{2\pi}\sum_\alpha \zeta_\alpha[\bar{\Psi}_{k,k_z,\alpha}\psi_k + \bar{\psi}_k\Psi_{k,k_z,\alpha}]. \tag{28}$$

Here, $\int_k \equiv \frac{1}{N_\Delta}\Sigma_{\mathbf{k}}\int\frac{d\omega}{2\pi}$, and $\tau_{\uparrow,\downarrow}$ are 2×2 matrices defined by

$$\tau_{\uparrow,\downarrow} = \begin{pmatrix} 1 & 0 \\ 0 & 0 \end{pmatrix}, \begin{pmatrix} 0 & 0 \\ 0 & 1 \end{pmatrix}. \tag{29}$$

Superscript K on various τ matrices indicates that they act in Keldysh space. $g_0^{R,A,K}(k)$ denote inverse retarded, advanced, and Keldysh Green's functions for noninteracting electrons in the graphene sheet while $\tilde{g}_\alpha^{R,A,K}(k)$ are the corresponding Green's functions for lead α. For the graphene sheet, they are given by

$$g_0^R(k) = \omega - \lambda_{\mathbf{k}} + i\delta = g_0^{A*}(k), \tag{30}$$

$$g_0^K(k) = 2i\delta K(\omega). \tag{31}$$

Here, $K(\omega) \equiv 1 + 2n_F(\omega)$ where $n_F(\omega)$ is the usual Fermi-Dirac distribution function. δ is an infinitesimal regularization parameter. For the noninteracting case, g_0^K merely serves as a regularization for the Keldysh functional integral. Because a finite self-energy term is anticipated from the coupling of graphene electrons to the leads, g_0^K can be safely omitted here (i.e., $g_0^K(k) \approx 0$).[19]

A. Integrating out the leads

We now integrate out the leads degrees of freedom in order to obtain an effective theory only in terms of fields defined on the graphene sheet. The inverse retarded, advanced, and Keldysh Green's functions for the leads, $\tilde{g}_\alpha^{R,A,K}$, are those corresponding to free fermions, and because the leads are always in thermal and chemical equilibrium, the Keldysh Green's function is strictly related to the retarded and advanced Green's functions via the fluctuation-dissipation theorem (FDT). They are given by

$$\tilde{g}_\alpha^R(k) = \omega - \epsilon_{\mathbf{k},k_z} + i\delta = g_\alpha^{A*}(k), \tag{32}$$

$$\tilde{g}_\alpha^K(k) = 2i\delta \tanh\left(\frac{\omega-\mu_\alpha}{2T}\right). \tag{33}$$

Upon integrating over the leads, the resulting self-energy action becomes

$$S_\Sigma = \int_k \bar{\psi}_k \{-\Sigma^R(k)\tau_z^N\tau_\uparrow^K - \Sigma^A(k)\tau_z^N\tau_\downarrow^K - \Sigma^K(k)\tau_\uparrow^N\tau_+^K - \Sigma^K(k)\tau_\downarrow^N\tau_-^K\}\psi_k, \tag{34}$$

where

$$\Sigma^R(k) = \sum_\alpha \int \frac{dk_z}{2\pi} \frac{\zeta_\alpha^2}{\omega - \epsilon_{\mathbf{k}} - \epsilon_{k_z} + i\delta} = -i\sum_\alpha \pi\rho t_\alpha^2 = -i\Gamma = \Sigma^{A*}(k) \tag{35}$$

and

$$\Sigma^K(k) = -2\pi i \sum_\alpha \int \frac{dk_z}{2\pi}\zeta_\alpha^2 \tanh\left(\frac{\omega-\mu_\alpha}{2T}\right)\delta(\omega - \epsilon_{\mathbf{k}} - \epsilon_{k_z}) = -2i\sum_\alpha \Gamma_\alpha \tanh\left(\frac{\omega-\mu_\alpha}{2T}\right). \tag{36}$$

Here, $\Gamma_\alpha \equiv \pi\rho t_\alpha^2$ measures the effective coupling strength between the layer and leads, and $\Gamma=\Gamma_L+\Gamma_R$. ρ is the lead density of states to tunnel into the layer assumed to be constant. The frequency-independent damping coefficient, Γ, and the vanishing real energy shift that result from our assumptions indicate that the bath is treated as an Ohmic environment.[22] Combining the actions in Eqs. (26) and (34), we obtain the dressed inverse Green's functions for electrons in the graphene sheet,

$$g^R(k) = \omega - \lambda_{\mathbf{k}} + i\Gamma = g^{A*}(k), \tag{37}$$

$$g^K(k) = 2i\sum_\alpha \Gamma_\alpha \tanh\left(\frac{\omega-\mu_\alpha}{2T}\right). \tag{38}$$

The negative imaginary part of $\Sigma^R(k)$ leads to an irreversible damping in the time-dependent Green's function $G^R(\mathbf{k},t)$. The damping term formally describes decoherence suffered by a propagating electron wave due to incoherent escape and injection of electrons into and from the leads.

At this point, it is convenient to shift the energy scale so that all energies are measured with respect to $\mu=(\mu_L+\mu_R)/2$. This is equivalent to the following mapping:

$$\omega \to \omega - \mu,$$

$$\lambda_{\mathbf{k}} \to \lambda_{\mathbf{k}} - \mu,$$

$$\mu_\alpha \to V_\alpha/2,$$

where $V_{L,R}=\pm V$ and $V\equiv\mu_L-\mu_R$. We assume $V>0$. Following this choice the inverse retarded Green's function [Eq. (37)] remains invariant while Eq. (38) becomes

$$g^K(k) = 2i\sum_\alpha \Gamma_\alpha \tanh\left(\frac{\omega-V_\alpha/2}{2T}\right). \tag{39}$$

Using the dressed inverse Green's functions defined in Eqs. (37) and (39), the effective action for the graphene sheet is

$$S_{\text{sys}}^{K,\text{eff}} = \int_k \bar{\psi}_k \mathcal{G}_k^{-1}\psi_k - 2U[\Delta_{cl}^*\Delta_q + \Delta_q^*\Delta_{cl}], \tag{40}$$

where the inverse Green's function matrix $\mathcal{G}_k^{-1}$ is now given by

$$\mathcal{G}_k^{-1} = \begin{pmatrix}
g^R(k) & \Delta_q & -g_{\mathbf{k}}^* & 0 & g^K(k) & \Delta_{cl} & 0 & 0 \\
\Delta_q^* & -g^R(-k) & 0 & g_{\mathbf{k}}^* & \Delta_{cl}^* & 0 & 0 & 0 \\
-g_{\mathbf{k}} & 0 & g^R(k) & \Delta_q & 0 & 0 & g^K(k) & \Delta_{cl} \\
0 & g_{\mathbf{k}} & \Delta_q^* & -g^R(-k) & 0 & 0 & \Delta_{cl}^* & 0 \\
0 & \Delta_{cl} & 0 & 0 & g^A(k) & \Delta_q & -g_{\mathbf{k}}^* & 0 \\
\Delta_{cl}^* & g^K(k) & 0 & 0 & \Delta_q^* & -g^A(-k) & 0 & g_{\mathbf{k}}^* \\
0 & 0 & 0 & \Delta_{cl} & -g_{\mathbf{k}} & 0 & g^A(k) & \Delta_q \\
0 & 0 & \Delta_{cl}^* & g^K(K) & 0 & g_{\mathbf{k}} & \Delta_q^* & -g^A(-k)
\end{pmatrix}. \tag{41}$$

B. Mean-field equations

In closed equilibrium, solutions to the mean-field gap and number equations on the honeycomb lattice have shown that while graphene exhibits a BCS-BEC crossover behavior away from the Dirac point for increasing attractive interaction strength, u, superconductivity in graphene at half filling requires a finite attractive interaction.[15,17] In this section, we derive the main results of our work which are the mean-field gap and number equations in the presence of leads and voltage. Solving these equations will allow us to study the effects of dissipation and nonequilibrium current on the gap as a function of attractive interaction strength u and filling n and compare the results to the equilibrium calculations. We begin by obtaining an effective theory for the s-wave order parameter alone by integrating out the graphene electrons. From Eq. (40), we obtain

$$iS^K_{\text{eff}}(\Delta,\Delta^*) = Tr\,\ln[-i\mathcal{G}_k^{-1}] - 2iU(\Delta^*_{cl}\Delta_q + \text{c.c.}). \quad (42)$$

1. Gap equation

The saddle-point analysis of the effective Keldysh action, Eq. (42), proceeds by taking functional derivatives of the action with respect to either of the two order-parameter fields defined in the Keldysh space. Extremizing with respect to the classical component and fixing the quantum component to zero yield a trivial relation which we do not pursue further. On the other hand, one may extremize with respect to the quantum component together with fixing the quantum component to zero (i.e., $\Delta_q=0$),

$$\left.\frac{\partial S^K_{\text{eff}}}{\partial \Delta^*_q}\right|_{\Delta_{cl}=\Delta,\Delta_q=0} = 0. \quad (43)$$

As we will show below, this yields a self-consistent equation for $\Delta_{cl}\equiv\Delta$. In the equilibrium limit, this equation reduces to the expected BCS gap equation. We therefore interpret the obtained nonequilibrium self-consistent equation for Δ to be the nonequilibrium analog of the equilibrium gap equation.

Difficulties in nonequilibrium mean-field analyses arise in general because the associated equations possess richer structure than the equilibrium counterparts, and one is often left with a series of possible solutions with no basis of knowing which of these solutions are relevant for the subsequent analysis. A resolution to this problem has been proposed in Ref. 23 for a model quantum dot system where features in the steady-state density matrix is used to select out the relevant solutions. From applying this analysis to the case of an extended system in a previous work,[21] we believe that the "classical"[19] saddle-point solution (i.e., $\Delta_q=0$) is in general a unique solution to the nonequilibrium mean-field equations for extended systems. In light of this observation, nonclassical saddle points with $\Delta_q\neq 0$ are not studied in this work.

Equation (43) yields

$$0 = \left.\frac{\partial S^K_{\text{eff}}}{\partial \Delta^*_q}\right|_{\Delta_q=0,\Delta_{cl}=\Delta} = -iTr\left\{\left.\frac{\tau^N_-}{\mathcal{G}_k^{-1}}\right|_{\Delta_q=0,\Delta_{cl}=\Delta}\right\} - \frac{2\Delta}{U}. \quad (44)$$

This equation leads to the generalized nonequilibrium gap equation,

$$\frac{2\Delta}{U} = \int_k \frac{4\Delta\omega\sum_\alpha \Gamma_\alpha \tanh\left(\frac{\omega - V_\alpha/2}{2T}\right)\{[(\omega+E_{\mathbf{k}})^2+\Gamma^2][(\omega-E_{\mathbf{k}})^2+\Gamma^2] + 4\lambda^2_{\mathbf{k}}|g_{\mathbf{k}}|^2\}}{\{[\omega-E_+(\mathbf{k})]^2+\Gamma^2\}\{[\omega-E_-(\mathbf{k})]^2+\Gamma^2\}\{[\omega+E_+(\mathbf{k})]^2+\Gamma^2\}\{[\omega+E_-(\mathbf{k})]^2+\Gamma^2\}}. \quad (45)$$

The spectra of the two bands are given by

$$E_\pm(\mathbf{k}) = \sqrt{\xi^2_\pm(\mathbf{k})+\Delta^2} \quad \xi_\pm(\mathbf{k}) = \lambda_{\mathbf{k}} \pm |g_{\mathbf{k}}|, \quad (46)$$

and $E_{\mathbf{k}}=\sqrt{\lambda^2_{\mathbf{k}}+|g_{\mathbf{k}}|^2+\Delta^2}$. After scaling all energies by bandwidth t and evaluating the ω integral we obtain

$$\frac{1}{u} = \frac{1}{2\pi N}\sum_{\mathbf{k}}\{F_v[\Xi_+(\mathbf{k})] + F_v[\Xi_-(\mathbf{k})]\}, \quad (47)$$

where

$$F_v(x) \equiv \frac{1}{x}\left[\tan^{-1}\left(\frac{\frac{v}{2}+x}{\gamma}\right) - \tan^{-1}\left(\frac{\frac{v}{2}-x}{\gamma}\right)\right],$$

and

$$\Xi_\pm(\mathbf{k}) = \frac{E_\pm(\mathbf{k})}{t}, \quad u = \frac{U}{t}, \quad \gamma_\alpha = \frac{\Gamma_\alpha}{t}, \quad v = \frac{V}{t}.$$

$\gamma=\gamma_L+\gamma_R$ denotes the sum of lead-graphene tunneling rates scaled by t. Equation (47) is the BCS gap equation in the presence of leads (γ) and voltage (v) and is the nonequilibrium generalization of Eq. 2 in Ref. 17. Indeed when one takes the limit as $\gamma\to 0$ and $v\to 0$ in Eq. (47), the equilibrium gap equation is recovered.

At low energies, excitations in graphene at or near half filling are concentrated near two inequivalent Fermi points at the corners of the hexagonal Brillouin zone. In the vicinity of these points, we have

$$\lambda_{\mathbf{k}} \approx 3t' - \mu \equiv m \quad |g_{\pm\mathbf{K}+\mathbf{k}}| \approx v_F|\mathbf{k}|, \quad (48)$$

where $v_F=3t/2$ is the Fermi velocity and $\pm\mathbf{K}=(\pm 4\pi/3\sqrt{3},0)$ are the locations of the inequivalent Fermi

points. Within this approximation, the quasiparticle dispersions, $\Xi_{\pm}(\mathbf{k})$, become

$$\xi_{\pm}(\mathbf{k}) \approx m \pm \epsilon \quad \Xi_{\pm}(\mathbf{k}) \approx \sqrt{\xi_{\pm}^2 + \Delta^2}, \tag{49}$$

where $\epsilon = v_F|\mathbf{k}|$. Noting that the area per lattice site is $A/N = 3\sqrt{3}/4$ the conversion from $\mathbf{k}$ summation to ϵ integral is given by

$$\frac{1}{N}\sum_{\mathbf{k}} = \frac{3\sqrt{3}}{4\pi v_F^2}\int_0^D \epsilon d\epsilon. \tag{50}$$

The energy cutoff, set by conserving the total number of states in the Brillouin zone, is $D = \sqrt{\sqrt{3}\pi} \approx 2.33$ in units of t. In the continuum limit, the gap equation then becomes

$$\frac{1}{u} = \frac{3\sqrt{3}}{8\pi^2 v_F^2}\int_0^D \epsilon d\epsilon \{F_v[\Xi_+(\mathbf{k})] + F_v[\Xi_-(\mathbf{k})]\}. \tag{51}$$

2. Number density equation

In equilibrium, the number density is computed using a thermodynamic relation $\partial \mathcal{F}_{\mathrm{MF}}/\partial \mu = -N_e$. Out of equilibrium, the relation does not hold and the particle density, n, must be extracted from one of the four Kadanoff-Baym Green's functions, $G^<$, using[24,25]

$$n = \frac{-i}{4}\sum_{\sigma,\Lambda}\int_k G^<_{\sigma,\Lambda}(k). \tag{52}$$

σ labels the electron spin and $\Lambda \in \{A, B\}$ labels the sublattice in which it propagates. In terms of Keldysh Green's functions,[19]

$$n = \frac{-i}{4}\sum_{\sigma,\Lambda}\int_k [G^K_{\sigma,\Lambda}(K) - G^R_{\sigma,\Lambda}(K) + G^A_{\sigma,\Lambda}(K)], \tag{53}$$

where $G^{R,A,K}(k)$ are the retarded, advanced, and Keldysh Green's functions for the graphene electrons. These Green's functions can be obtained by inverting the matrix, $\mathcal{G}^{-1}(k)$, in Eq. (41). We find that the form of the Green's functions is independent of spin and sublattice, and the resulting number equation reads

$$n = \frac{4\gamma}{N}\sum_{\mathbf{k}}\int \frac{d\omega}{2\pi}\frac{[1 - F(\omega,v)](c_6\omega^6 + c_5\omega^5 + c_4\omega^4 + c_3\omega^3 + c_2\omega^2 + c_1\omega + c_0)}{[(\omega + \Xi_+)^2 + \gamma^2][(\omega + \Xi_-)^2 + \gamma^2][(\omega - \Xi_+)^2 + \gamma^2][(\omega - \Xi_-)^2 + \gamma^2]}. \tag{54}$$

$F(\omega, v)$ is the zero-temperature nonequilibrium electron distribution and is given by

$$F(\omega,v) = \sum_{\alpha}\frac{\gamma_\alpha}{\gamma}\mathrm{sgn}(\omega - v_\alpha) = \frac{\gamma_L}{\gamma}\mathrm{sgn}\left(\omega - \frac{v}{2}\right) + \frac{\gamma_R}{\gamma}\mathrm{sgn}\left(\omega + \frac{v}{2}\right). \tag{55}$$

An exact evaluation of the ω integral in Eq. (54) is difficult. However, it can be done in the limit where the applied bias is assumed small compared to the bandwidth and the dampling coefficient, i.e., $v \ll \min\{1, \gamma\}$. Computing the integral up to quadratic order in v the number density yields

$$\begin{aligned} n = {} & \frac{3\sqrt{3}}{4\pi v_F^2}\int_0^D \epsilon d\epsilon \frac{c_0(10\gamma^2 + \Xi_+^2 + \Xi_-^2) + (\gamma^2 + \Xi_+^2)(\gamma^2 + \Xi_-^2)[2c_2 + c_4(2\gamma^2 + \Xi_+^2 + \Xi_-^2) + c_6(10\gamma^4 + 6\gamma^2\Xi_-^2 + \Xi_-^4 + 6\gamma^2\Xi_+^2 + \Xi_+^4)]}{(\gamma^2 + \Xi_+^2)(\gamma^2 + \Xi_-^2)[16\gamma^4 + \Xi_+^2(8\gamma^2 + \Xi_+^2 - \Xi_-^2) + \Xi_-^2(8\gamma^2 + \Xi_-^2 - \Xi_+^2)]} \\ & - \frac{2}{\pi[(\Xi_+^2 - \Xi_-^2)^3 + 8\gamma^2\Xi_+^2(2\gamma^2 + \Xi_+^2) - 8\gamma^2\Xi_-^2(2\gamma^2 + \Xi_-^2)]}\Bigg\{\frac{\tan^{-1}\left(\frac{\Xi_+}{\gamma}\right)}{\Xi_+}\{c_1(\Xi_+^2 - \Xi_-^2 - 4\gamma^2) + c_3[\Xi_+^4 + \gamma^2\Xi_-^2 + 4\gamma^4 - \Xi_+^2(\Xi_-^2 \\ & - 3\gamma^2)] + c_5[\Xi_+^6 + 6\gamma^2\Xi_+^4 + 9\gamma^4\Xi_+^2 - \Xi_-^2(\gamma^4 - 6\gamma^2\Xi_+^2 + \Xi_+^4) - 4\gamma^6]\} - (- \leftrightarrow +) + \gamma \ln\left(\frac{\gamma^2 + \Xi_+^2}{\gamma^2 + \Xi_-^2}\right)[2c_1 + c_3(\Xi_+^2 + \Xi_-^2 + 2\gamma^2) \\ & + 2c_5(\Xi_+^2\Xi_-^2 - \gamma^2\Xi_+^2 - \gamma^2\Xi_-^2 - 3\gamma^4)]\Bigg\} + (2x - 1)\frac{2\gamma c_0}{\pi(\gamma^2 + \Xi_+^2)^2(\gamma^2 + \Xi_-^2)^2}v + \frac{\gamma c_1}{2\pi(\gamma^2 + \Xi_+^2)^2(\gamma^2 + \Xi_-^2)^2}v^2, \end{aligned} \tag{56}$$

where $x = \gamma_L/\gamma$ and $\Xi_{\pm}$ are given by Eq. (49). The coefficients $c_0, \ldots, c_6$ are dependent on $\Xi_{\pm}$, $\xi_{\pm}$, and γ and are defined as

$$c_6 = 1,$$

$$c_5 = \xi_+ + \xi_-,$$

$$c_4 = 3\gamma^2 - \frac{\Xi_+^2 + \Xi_-^2}{2},$$

$$c_3 = 2[\xi_+(\gamma^2 - \Xi_-^2) + \xi_-(\gamma^2 - \Xi_+^2)],$$

$$c_2 = 3\gamma^4 + (\Xi_+^2 - \Xi_-^2)^2 + \gamma^2(\Xi_-^2 + \Xi_+^2) - \frac{\Xi_-^4}{2} - \frac{\Xi_+^4}{2},$$

$$c_1 = \xi_-(\gamma^4 + 2\gamma^2\Xi_+^2 + \Xi_+^4) + \xi_+(\gamma^4 + 2\gamma^2\Xi_-^2 + \Xi_-^4),$$

$$c_0 = \frac{1}{2}(\Xi_-^2 + \gamma^2)(\Xi_+^2 + \gamma^2)(\Xi_+^2 + \Xi_-^2 + 2\gamma^2). \quad (57)$$

It can be easily verified that in the limit of $\gamma \to 0$ and $v \to 0$, Eq. (56) reduces to the equilibrium number equation (cf. Eq. 3 in Ref. 17). The mean-field equations in Eqs. (51) and (56) are the central results of this work. These equations will be analyzed in the remainder of the paper.

IV. RESULTS

Our main focus will be on obtaining and analyzing gap phase diagrams in the parameter space of interaction strength (u) and number density (n) for various leads-graphene couplings (γ_L, γ_R) and external biases (v). A previous work on closed equilibrium graphene[17] revealed that at half filling, the superconducting instability of the semimetallic phase requires a critical attractive interaction strength u_c, and thus, the gap vanishes up to u_c. Away from half filling, the metallic phase is immediately unstable to superconductivity for arbitrarily weak attractive interaction strength. As a result, the gap remains finite for any finite u and the system displays a typical BCS-BEC crossover behavior. In this section we quantitatively discuss the effects of dissipation and nonequilibrium current on the gap phase diagram by numerically solving the generalized mean-field equations [Eqs. (51) and (56)]. Sections IV A 1 and IV A 2 will show that a dramatic modification to the phase diagram is observed by the mere coupling of graphene to its environment even in the absence of nonequilibrium current. We find that the effects of external biases in addition to dissipation do not substantially alter the qualitative features of the phase diagram from the case in which the system is subject to dissipation alone. However, as Sec. IV B will discuss, the application of an external bias leads to shifts in the metallic region surrounding half filling which result from voltage-induced changes in the graphene electron density. The results presented here are applicable to the case of small biases ($v \ll \min\{1, \gamma\}$); effects of large biases are not considered here.

A. Finite lead-layer coupling $\gamma \neq 0$ with zero voltage ($v=0$)

First, we begin with the case in which the lead-graphene-lead heterostructure is in thermodynamic equilibrium. In particular, this is the situation where $\mu_L = \mu_R = \mu_{\text{res}}$, and in the long-time limit $\mu_{\text{sys}} = \mu_{\text{res}}$ is maintained. Here, electron-tunneling processes between the central graphene system and the leads are providing a mechanism for decoherence for the particles in the system ($\gamma \neq 0$), but an external bias that explicitly breaks time-reversal symmetry of the heterostructure is absent ($v=0$). Consider the case where the central graphene sheet is in a superconducting phase. Because of its coupling to the leads one can envisage a situation in which an electron that constitutes a Cooper pair escapes into the leads. Because the leads are assumed to be infinite the electron that has escaped the system is completely lost in the leads and as a consequence looses its coherence with its former partner. Although a different electron may enter the system from a lead within a time scale of $\tau_{\text{tun}} \sim 1/\Gamma$, the electron will not necessarily pair with the widowed electron since it completely lacks coherence to do so. Because dissipation effectively acts as a pair-breaking mechanism we expect a suppression of the gap throughout the entire region of the phase diagram.

Figure 5 plots the gap phase diagrams for various leads-graphene coupling strengths (γ). Figure 5(a) corresponds to the closed equilibrium case which has been obtained previously.[17] Figures 5(b) and 5(c) display the behavior of the gap as γ is increased. It is apparent from these plots that the suppressed region in the gap (dark blue region) grows as γ is strengthened. Regions of large gap values corresponding to the region with large u also display an overall suppression in the gap as γ is increased. The qualitative features of the diagrams are consistent with the expectation described above. Let us now discuss the results more quantitatively.

1. Half filling ($n=1$)

For the closed equilibrium case at half filling ($\gamma = v = 0$ and $n=1$) the semi-metal-superconductor transition is possible mainly because the divergent nature of the integral on the right-hand side of Eq. (51) is cured by particle-hole symmetry. When the integral is convergent, it is clear that a solution to the gap equation does not exist for small u where u^{-1} becomes larger than the integral. The value of the critical interaction parameter at which the transition occurs can be easily quantified. At half filling the number equation, Eq. (56), is satisfied by $m = 3t' - \mu = 0$, and thus, at the critical point ($n=1$, $\Delta=0$, and $m=0$) the gap equation reads

$$\frac{1}{u_c} = \frac{3\sqrt{3}}{4\pi v_F^2}\int_0^D d\epsilon = \frac{1}{2.33}. \quad (58)$$

For any $u < u_c$ the equations cannot be solved with any real Δ and the system enters the semimetallic phase. In the presence of dissipation ($\gamma > 0$) the number equation is still solved by $m=0$ at half filling, and the gap equation at the critical point yields

$$\frac{1}{u_c} = \frac{3\sqrt{3}}{2\pi^2 v_F^2}\int_0^D d\epsilon \tan^{-1}\left(\frac{\epsilon}{\gamma}\right)$$

$$= \frac{3\sqrt{3}D}{2\pi^2 v_F^2}\left[\tan^{-1}(\gamma_D^{-1}) - \frac{\gamma_D}{2}\ln(1+\gamma_D^{-2})\right], \quad (59)$$

where the reduced coupling strength is given by $\gamma_D = \gamma/D$.

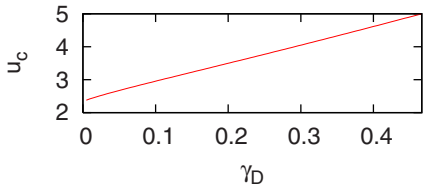

FIG. 4. (Color online) The plot of critical coupling u_c as a function of reduced leads-graphene coupling $\gamma_D = \gamma/D$.

The integral on the right-hand side of Eq. (59) is convergent, and thus, tells us that the semi-metal-superconductor transition exists in the presence of dissipation at half filling. The behavior of u_c as a function of γ_D is plotted in Fig. 4. We see that the value of u_c increases as γ is increased. This is consistent with the above considerations from which we expect that a larger interaction parameter is necessary to achieve pairing since leads-induced decoherence generally suppresses superconductivity. The phenomenon can also be observed in Fig. 5 where the apex of the blue region shifts right for larger γ. The plots show that at $\gamma=0$ u_c converges to the closed equilibrium value of $u_c \sim 2.33$ as predicted by previous calculations.

2. *Away from half filling* ($n \neq 1$)

In the closed equilibrium case away from half filling, $m \neq 0$ and the critical-point condition becomes

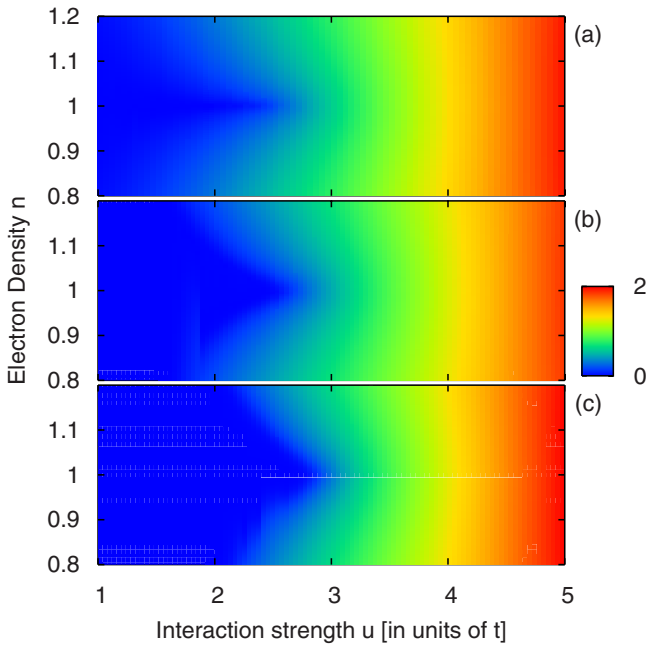

FIG. 5. (Color online) Plots of the BCS gap, Δ, in the parameter space of attractive interaction strength u and electron density n. The three diagrams correspond to different values of leads-graphene coupling strengths. In (a), the system is closed, i.e., $\gamma=0$, while in (b) and (c), $\gamma=0.1$ and 0.2, respectively. As the coupling is increased, the blue region in the phase diagram where the gap is small grows. In parts of the blue regions in (b) and (c) the gap is zero even for $n \neq 1$, indicating that a metal-superconductor quantum phase transition emerges in the presence of dissipation.

$$\frac{1}{u_c} = \frac{3\sqrt{3}}{4\pi v_F^2}\int_0^D \epsilon d\epsilon \left[\frac{1}{|m+\epsilon|} + \frac{1}{|m-\epsilon|}\right] = \infty. \tag{60}$$

The divergence of the integral results in a solution with $\Delta > 0$ for any small $u > 0$. This gives $u_c = 0$ implying that Cooper instability occurs for any finite u away from half filling. Let us now investigate how this is modified when γ is finite.

What is notable in Fig. 5 is the expansion of the blue region, where the gap is small, as γ is increased. The question is whether or not the typical BCS-BEC crossover behavior observed in the closed equilibrium case is a correct physical picture away from half filling for finite γ. The external baths acting as a pair-breaking mechanism make the issue subtle. The pair-breaking perturbation in a superconductor with magnetic impurities has been shown[26,27] to strongly suppress the transition temperature of the superconductor. Therefore, when such perturbation is strong enough the gap may vanish completely and gives rise to a metal-superconductor quantum phase transition at finite doping. The question of whether or not the gap vanishes away from half filling depends on the convergence of the integral in the gap equation. At $v=0$, the generalized gap equation becomes

$$\frac{1}{u} \propto \int_0^D \epsilon d\epsilon \left[\frac{1}{\Xi_+}\tan^{-1}\left(\frac{\Xi_+}{\gamma}\right) + (+ \rightarrow -)\right]. \tag{61}$$

We see that for any m (i.e., regardless of being at half filling or not), the integral is convergent because for any small $\Xi_\pm$, which is the source of divergence, the arctangent factor nullifies the divergence. This implies a finite u_c at both half filling and away from half filling. Consequently, the system should undergo a superconductor-to-metal phase transition as the interaction parameter is lowered. Notice that the analysis above infers that the system will eventually enter the metallic phase as u is decreased for any density.

Figure 6 explicitly shows regions in the gap phase diagram where the gap equation lacks a solution with any positive Δ. The diagrams are plotted for the same values of γ as in Fig. 5. The black regions are where the gap equation is solutionless and represent a (semi) metallic phase. Clearly, as γ is increased, the metallic region expands. We find that the superconducting (white) and metallic (black) regions are separated by a second-order phase transition.

The emergence of this dissipation-induced metal-superconductor quantum phase transition is not a peculiar consequence of the relativistic nature of the quasiparticles in graphene. A similar result is obtained for an ordinary BCS system with Schrödinger fermions. In this case, a single-band form of the gap equation in Eq. (47) obtained with the dispersion in the formula replaced by the usual quadratic form,

$$\frac{1}{U} = \frac{1}{N}\sum_{\mathbf{k}} \frac{1}{\pi E_{\mathbf{k}}}\tan^{-1}\left(\frac{E_{\mathbf{k}}}{\Gamma}\right), \tag{62}$$

where

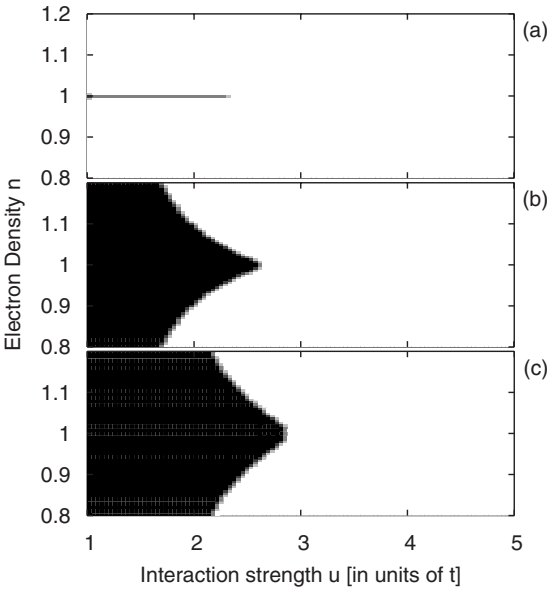

FIG. 6. The dark areas above show regions in the phase diagram where the gap equation lacks a solution for any finite Δ; the gap vanishes in these regions. As in Fig. 5, the system is closed for plot (a) while $\gamma=0.1$ and 0.2 in plots (b) and (c), respectively.

$$E_{\mathbf{k}} = \sqrt{(\epsilon_{\mathbf{k}} - \mu)^2 + \Delta^2} \quad \epsilon_{\mathbf{k}} = \frac{k^2}{2m}.$$

At $\Delta=0$, where the integral is maximized, we get

$$\frac{1}{U_c} = \frac{Am}{2\pi^2 N}\int_{\mu-\Lambda}^{\mu+\Lambda} \frac{d\epsilon}{|\epsilon-\mu|}\tan^{-1}\left(\frac{|\epsilon-\mu|}{\Gamma}\right)$$
$$= \frac{Am}{2\pi^2 N}\int_{-\Lambda}^{\Lambda} \frac{dx}{|x|}\tan^{-1}\left(\frac{|x|}{\Gamma}\right). \tag{63}$$

This integral is convergent for any finite $\Gamma>0$. But at $\Gamma=0$ the integral diverges signifying that Cooper instability occurs for any finite attractive U.

B. Effect of voltage ($v \neq 0$)

So far, we have discussed the effect of leads-induced dissipation on the gap phase diagram in the absence of voltage. We now consider the effects of driving an out-of-plane charge current through the superconducting graphene sheet. Here, we are limited to a regime of small voltages, specifically $v \ll \min\{1, \gamma\}$. As mentioned before, we assume $v \propto \mu_L - \mu_R > 0$ and allow asymmetric couplings of the lead-layer couplings γ_L and γ_R. In the absence of current ($v=0$), the gap equation depends only on the sum of these couplings $\gamma=\gamma_L+\gamma_R$. But Eq. (56) shows that in the presence of current ($v \neq 0$) the number density depends on these couplings independently, and depending on the relative strengths of these couplings the dominant correction term may change sign. The main qualitative modifications to the gap phase diagram in the presence of finite voltage reflect the influence of this correction term.

In the small voltage regime and for $\gamma<1$, the dominant correction term gives a correction of order $\gamma v \ll 1$ to the number density, which is of order unity. Because the modifications to the gap phase diagram due to voltage are expected to be small we present a cartoon representation of how it affects the boundary of the metallic region (black region in Fig. 6). This is shown in Fig. 7. Modifications to the metallic region of the phase diagram are plotted here for $\gamma_L > \gamma_R$ in Fig. 7(a) and $\gamma_L < \gamma_R$ in Fig. 7(b). The plots reveal that the metallic region (also the dark blue regions in Fig. 5) shifts vertically away from half filling. For $\gamma_L > \gamma_R$ the apex shifts up while for $\gamma_L < \gamma_R$ it shifts down. Given that $\mu = (\mu_L + \mu_R)/2$ and $v>0$, the lowest-order voltage correction in Eq. (56) tells us that the number density increases or decreases depending on the asymmetry of the lead couplings. If $\gamma_L > \gamma_R$, n increases, while if $\gamma_L < \gamma_R$, n decreases. The gap equation yields the largest value of u_c given by γ and v when $m=0$. Thus, the above observation tells us that for $\gamma_L > \gamma_R$, $m=0$ is achieved not at half filling as in the equilibrium case but at $n>1$. This shifts the apex upward. The opposite occurs for $\gamma_L < \gamma_R$. The nonequilibrium gap equation is convergent for all μ; thus, a metallic phase is once again expected at all densities.

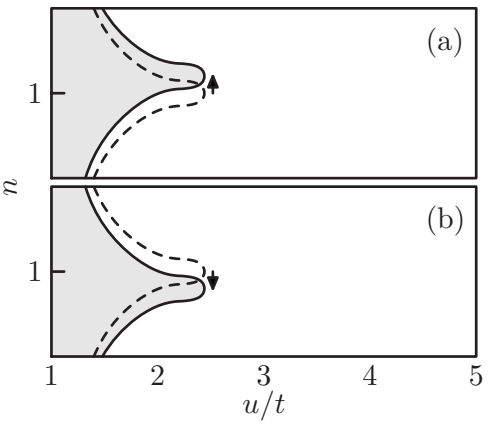

FIG. 7. A cartoon plot showing the effect of voltage on the boundary of the metallic region. The dashed lines in both plots denote the boundary at $v=0$. The shaded area is the metallic region after a steady-state bias is applied. In both plots, the applied voltage is $v=0.1$. However, $\gamma_L > \gamma_R$ in (a) while $\gamma_L < \gamma_R$ in (b). Essentially, the voltage-induced modification is to shift the metallic region to higher values in density or to lower values depending on the polarity of the voltage and the lead-coupling asymmetry.

V. CONCLUSION

In conclusion, we have theoretically studied the effects of dissipation and nonequilibrium drive on the properties of superconducting graphene. An external steady-state current was perpendicularly driven through the graphene sheet by attaching it to two leads which were equilibrated at two constant but different chemical potentials. The mean-field BCS theory of superconductivity on graphene was extended to the nonequilibrium situation by formulating the theory on the Keldysh contour. After obtaining nonequilibrium gap and number density equations we studied the BCS gap as a function of attractive interaction strength u and electron density n for various lead-graphene coupling strengths γ and voltages

v. We have shown that dissipation results in a suppression of the BCS gap at both zero and finite voltages. We argued that the coupling of the graphene sheet to external baths acts as a pair-breaking mechanism because it causes an electron that constitutes a Cooper pair to escape into the leads. Once an electron leaves the scattering region, it looses coherence with its time-reversed partner and the destruction of the Cooper pair entails.

A quantitative understanding of why the gap is significantly suppressed by dissipation can be gained by observing how dissipation affects the gap equation. Recall that the BCS gap equation for an ordinary superconductor[28] in closed equilibrium is given by

$$\Delta = uTN(0)\sum_n \frac{\Delta}{\sqrt{\omega_n^2 + \Delta^2}}. \tag{64}$$

$N(0)$ is the density of states at the Fermi energy, and $u>0$ is the attractive interaction strength. A general result for these ordinary superconductors is that the gap equation [Eq. (64)], and hence the gap, is unaffected by time-reversal-invariant perturbations. Take, for example, the influence of nonmagnetic impurities on the superconducting state. The gap equation obtained after invoking disorder averaging and the Born approximation reads

$$\Delta = uT\tilde{N}(0)\sum_n \frac{\tilde{\Delta}}{\sqrt{\tilde{\omega}_n^2 + e\tilde{\Delta}^2}}, \tag{65}$$

where $\tilde{\omega}$ and $\tilde{\Delta}$ are frequency and order parameter renormalized by the perturbation,[29–31] and $\tilde{N}(0)$ is the density of states in the presence of the perturbation. The essential point is that $\tilde{\omega}$ and $\tilde{\Delta}$ are related to their unrenormalized counterparts by a common factor $\eta = \eta(\omega_n, \Delta)$, i.e.,

$$\tilde{\omega} = \eta\omega,$$

$$\tilde{\Delta} = \eta\Delta.$$

Because this factor η cancels out in Eq. (65), the gap equation remains invariant and leads to the result that the gap is unaffected by nonmagnetic impurities.[32]

Imagine now that a pure ordinary superconductor is coupled to an external bath in equilibrium. The Nambu-Gorkov equations can be straightforwardly derived for this case,

$$[i\omega_n + i\ \mathrm{sgn}(\omega_n)\Gamma - \xi_{\mathbf{k}}]G + \Delta F = 1, \tag{66}$$

$$[i\omega_n + i\ \mathrm{sgn}(\omega_n)\Gamma + \xi_{\mathbf{k}}]F + \Delta G = 0, \tag{67}$$

where the ordinary and anomalous Green's functions are given by

$$G(\mathbf{k}, \omega_n) = -\int_0^\beta d\tau \langle T_\tau c_{\mathbf{k},\uparrow}(\tau) c^\dagger_{\mathbf{k},\uparrow}(0)\rangle e^{i\omega_n\tau},$$

$$F(\mathbf{k}, \omega_n) = -\int_0^\beta d\tau \langle T_\tau c_{\mathbf{k},\uparrow}(\tau) c_{-\mathbf{k},\downarrow}(0)\rangle e^{i\omega_n\tau}.$$

We immediately see from Eqs. (66) and (67) that ω and Δ scale asymmetrically, namely,

$$\tilde{\omega} = \eta\omega, \quad \tilde{\Delta} = \Delta; \quad \eta = 1 + \frac{\Gamma}{|\omega_n|}. \tag{68}$$

Here, Γ is the rate at which electrons decay into the bath. The asymmetry in the renormalization of ω and Δ [Eq. (68)] greatly affects the gap equation, Eq. (65), and shows how dissipation can affect the gap significantly. This is consistent with the qualitative argument given above.

We believe the observed features in the gap phase diagram (Figs. 5 and 6) to be robust even in the presence of fluctuation effects. Indeed, fluctuation effects are expected to be important only near the critical point.[21,33] Renormalization group treatment of these fluctuations in the vicinity of the metal-superconductor quantum critical point is a topic that we are currently addressing. Results from this work may shift the boundaries of the transition and modify scaling properties near the transition. However, the gap phase diagram presented in this work is nevertheless expected to be valid at a qualitative level.

We also expect the phenomenon of dissipation-induced suppression of the gap to occur in cases where the geometry of the system has more relevance to actual experimental setups. In particular, we have verified in equilibrium that the phenomenon persists even for a graphene sheet placed on top of a single substrate with which it exchanges particles. In the context of itinerant electron magnets,[21,33] nonequilibrium renormalization-group analysis showed that the critical properties of the system near its ferromagnet-paramagnet quantum critical point are impervious to the change in geometry

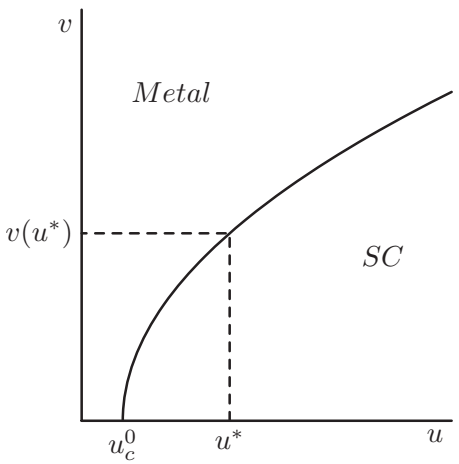

FIG. 8. A plot of u_c vs v for a fixed μ. The plot line separates the metallic and superconducting phases of our system. Adjusting μ will tune the location of u_c^0 on the x axis but the general shape of the curve is not modified.

with which the nonequilibrium drive is applied to the system. In light of these works and our analysis, we expect our qualitative results to hold both in and out of equilibrium even when the system geometry is altered to the more experimentally accessible configuration mentioned above.

The emergence of the metal-superconductor quantum phase transition in the graphene subsystem at both zero and finite voltages gives rise to the possibility of inducing the phase transition using external bias. While fixing the average chemical potential μ to some value, v can be changed by adjusting μ_L and μ_R symmetrically about μ. u_c is obtained from the gap equation in this situation by fixing $\Delta=0$ and μ to some value. Figure 8 shows a generic plot of u_c as a function of voltage. If the interaction strength, u, of the system is at $u=u^*$, then for $v<v(u^*)$ the system will be metallic. However, when v is increased and passes $v=v(u^*)$, the system will become superconducting. u_c^0 can be tuned by adjusting the average chemical potential μ. It is clear from Eq. (56) that when the average chemical potential μ is fixed, the electron density can change as a function of voltage.

This voltage-induced metal-superconductor quantum phase transition in open nonequilibrium graphene is possible when u_c^0 in Fig. 8 is less than the attractive interaction strength u^* so that voltage can be increased to drive the system from the superconducting phase to the metallic phase. An estimate for u^* can be made within the weak-coupling limit using[15]

$$u^* = \frac{u_c(\gamma=0)}{1-\frac{m}{D}\left[1+\ln\left(\frac{T_c\pi}{1.154m}\right)\right]}. \tag{69}$$

Equation (69) was obtained in the context of closed equilibrium graphene and may not be an accurate estimate for u^* in the presence of external leads. Nevertheless, we use this estimate in conjunction with the assumption of weak lead-layer coupling $\gamma\sim 0.001$. Adjusting the average chemical potential of the leads at $m\sim 0.2t$ and estimating the critical temperature from those of graphite intercalated compounds,[34,35] i.e., $T_c\sim 10$ K, we obtain $u^*\approx 1.56t$ and $u_c^0\approx 1.47t$. The system then is initially in the superconducting phase and enters the metallic phase with the application of voltage.

ACKNOWLEDGMENTS

The authors would like to thank Michael Lawler, Eun-Ah Kim, Erhai Zhao, Arun Paramekanti, and Ilya Vekhter for helpful discussions. This research was supported by NSERC (S.T.), The Canada Research Chair program, Canadian Institute for Advanced Research, and Korea Research Foundation through KRF-2005-070-C00044 (Y.B.K.).

[1] K. S. Novoselov, A. K. Geim, S. V. Morozov, D. Jiang, Y. Zhang, S. V. Dubonos, I. V. Grigorieva, and A. A. Firsov, Science **306**, 666 (2004).
[2] K. S. Novoselov, D. Jiang, F. Schedin, T. J. Booth, V. V. Khotkevich, S. V. Morozov, and A. K. Geim, Proc. Natl. Acad. Sci. U.S.A. **102**, 10451 (2005).
[3] A. K. Geim and K. S. Novoselov, Nat. Mater. **6**, 183 (2007), and references therein.
[4] A. H. Castro Neto, F. Guinea, N. M. R. Peres, and A. K. Geim, arXiv:0709.1163, Rev. Mod. Phys. (to be published).
[5] G. W. Semenoff, Phys. Rev. Lett. **53**, 2449 (1984).
[6] E. Fradkin, Phys. Rev. B **33**, 3263 (1986).
[7] F. D. M. Haldane, Phys. Rev. Lett. **61**, 2015 (1988).
[8] K. S. Novoselov, A. K. Geim, S. V. Morozov, D. Jiang, M. I. Katsnelson, I. V. Grigorieva, S. V. Dubonos, and A. A. Firsov, Nature (London) **438**, 197 (2005).
[9] Y. Zhang, J. W. Tan, H. L. Stormer, and P. Kim, Nature (London) **438**, 201 (2005).
[10] F. Schedin, A. K. Geim, S. V. Morozov, E. W. Hill, P. Blake, M. I. Katsnelson, and K. S. Novoselov, Nat. Mater. **6**, 652 (2007).
[11] B. Özyilmaz, P. Jarillo-Herrero, D. Efetov, D. A. Abanin, L. S. Levitov, and P. Kim, Phys. Rev. Lett. **99**, 166804 (2007).
[12] M. C. Lemme, T. J. Echtermeyer, M. Baus, and H. Kurz, IEEE Electron Device Lett. **28**, 282 (2007).
[13] B. Huard, J. A. Sulpizio, N. Stander, K. Todd, B. Yang, and D. Goldhaber-Gordon, Phys. Rev. Lett. **98**, 236803 (2007).
[14] H. B. Heersche, P. Jarillo-Herrero, J. B. Oostinga, L. M. K. Vandersypen, and A. F. Morpurgo, Nature (London) **446**, 56 (2007).
[15] B. Uchoa and A. H. Castro Neto, Phys. Rev. Lett. **98**, 146801 (2007).
[16] A. Bostwick, T. Ohta, T. Seyller, K. Horn, and E. Rotenberg, Nat. Phys. **3**, 36 (2007).
[17] E. Zhao and A. Paramekanti, Phys. Rev. Lett. **97**, 230404 (2006).
[18] S. Reich, J. Maultzsch, C. Thomsen, and P. Ordejón, Phys. Rev. B **66**, 035412 (2002).
[19] A. Kamenev, arXiv:cond-mat/0412296 (unpublished).
[20] S. Takei and Y. B. Kim, Phys. Rev. B **76**, 115304 (2007).
[21] A. Mitra, S. Takei, Y. B. Kim, and A. J. Millis, Phys. Rev. Lett. **97**, 236808 (2006).
[22] U. Weiss, *Quantum Dissipative Systems* (World Scientific, Singapore, 1999).
[23] A. Mitra, I. Aleiner, and A. J. Millis, Phys. Rev. Lett. **94**, 076404 (2005).
[24] L. P. Kadanoff and G. Baym, *Quantum Statistical Mechanics* (Benjamin, Reading, 1962), Chap. 2.
[25] G. D. Mahan, *Many-Particle Physics* (Plenum, New York, 1990), Chap. 3.
[26] A. A. Abrikosov and L. P. Gorkov, Zh. Eksp. Teor. Fiz. **39**, 1781 (1960) [Sov. Phys. JETP **12**, 1243 (1961)].
[27] B. T. Matthias, H. Suhl, and E. Corenzwit, Phys. Rev. Lett. **1**, 92 (1958); J. Phys. Chem. Solids **13**, 156 (1959).
[28] Here, we are considering an ordinary Fermi liquid (with quadratic dispersion relation) in the BCS superconducting phase.
[29] See K. Maki, *Superconductivity*, edited by R. D. Parks (Dekker, New York, 1969), Vol. II, and references therin.
[30] M. Crisan, *Theory of Superconductivity* (World Scientific, New

Jersey, 1989) Chap. 30.16.
[31] A. A. Abrikosov, L. P. Gorkov, and I. E. Dzyaloshinski, *Methods of Quantum Field Theory in Statistical Physics* (Dover, New York, 1963), Chap. 39.3.
[32] A. A. Abrikosov and L. P. Gorkov, Sov. Phys. JETP **8**, 1090 (1959).
[33] A. Mitra and A. J. Millis, Phys. Rev. B **77**, 220404(R) (2008).
[34] G. Lamura, M. Aurino, G. Cifariello, E. Di Gennaro, A. Andreone, N. Emery, C. Hrold, J. F. March, and P. Lagrange, Phys. Rev. Lett. **96**, 107008 (2006).
[35] I. I. Mazin, Phys. Rev. Lett. **95**, 227001 (2005).